INTERNATIONAL JOURNAL OF CHEMICAL REACTOR ENGINEERING

Flow Generated by Radial Flow Impellers: PIV Measurements and CFD Simulations

Avinash Khopkar[*]   Joella Aubin[†]   C Rubio-Atoche[‡]

Catherine Xuereb[**]   Nathalie Le Sauze[††]

Joel Bertrand[‡‡]   Vivek V. Ranade[§]

[*]National Chemical Laboratory, arkhopkar@ifmg.ncl.res.in

[†]ENSIACET, Joelle.Aubin@ensiacet.fr

[‡]ENSIACET, Rubio-Atoche@ensiacet.fr

[**]ENSIACET, Catherine.Xuereb@ensiacet.fr

[††]ENSIACET, nathalie.lesauze@iut-tlse3.fr

[‡‡]ENSIACET, Joel.Bertrand@ensiacet.fr

[§]National CHemical Laboratory, vvranade@ifmg.ncl.res.in

Flow Generated by Radial Flow Impellers: PIV Measurements and CFD Simulations

Avinash Khopkar, Joella Aubin, C Rubio-Atoche, Catherine Xuereb, Nathalie Le Sauze, Joel Bertrand, and Vivek V. Ranade

Abstract

Particle image velocimetry (PIV) and computational fluid dynamics (CFD) have been used to investigate the single phase and gas-liquid flow generated by a Scaba SRGT turbine. The key details of the trailing vortices, the turbulent flow around the impeller blades and the accumulation of gas have been studied by using PIV measurements and CFD simulations. Both the experimental and numerical results show that the flow and the trailing vortices are not altered significantly upon gassing. The simulated results are generally in good agreement with the experimental findings. The CFD simulations also show that only small low-pressure regions exist behind the blades of the Scaba turbine compared with the very large low-pressure zones formed by the Rushton turbine. These results enable better understanding of the improved performance of the Scaba turbine for gas-liquid dispersions compared with the Rushton turbine.

KEYWORDS: Stirred vessel, Gas-liquid flow, Scaba turbine, Rushton turbine, PIV, CFD

1. INTRODUCTION

Stirred vessels are widely used in the process industry to carry out gas-liquid reactions. In most of the process applications, the Rushton turbine is widely used for dispersing gas in the liquid bulk. For this impeller, the sparged gas interacts with trailing vortices present behind the impeller blades and accumulates in a vortex core region of trailing vortices. This gas accumulation forms gas pockets behind the impeller blades, which are also known as gas cavities. These gas cavities significantly reduce the pumping capacity and the power dissipated by the impeller, therefore having negative effects on the performance of the stirred vessel (Bruijn et al., 1974). Since the discovery of these inherent problems of the Rushton turbine, there has been constant interest to improve the performance of aerated stirred vessels by modifying the impeller blade shape. Van't Riet et al. (1976) observed a remarkable improvement in the loss of power draw under aeration by replacing the six flat blades of the Rushton turbine with six half-pipe segments (Smith turbine). This change in blade shape modifies the structure of the trailing vortices and reduces their strength. This in turn reduces the extent of gas accumulation behind impeller blades.

The blade shape proposed by Van't Riet et al. (1976) was considered as the initial design of the Scaba Radial Flow Gas Dispersing Turbine (6SRGT). The experimental study carried out by Saito et al. (1992) shows the excellent capability of the Scaba turbine to disperse gas. At an equivalent power input and impeller size, the Scaba turbine handles approximately three times as more gas compared with the Rushton turbine before the loaded condition changes to the flooded regime. Also, the ratio of the aerated power to the non-aerated power of the Scaba turbine does not drop upon gassing and remains close to one (Saito et al., 1992). The efficient gas dispersion capability of the Scaba turbine was linked with the cavity structure developed behind the impeller blades. Similar to the Rushton turbine (Nienow et al., 1977 and Nienow, 1990), the Scaba turbine also supports the ventilated cavities of different shapes. Saito et al. (1992) defined three cavity structures, viz. vortex clinging, 3-3 (3 vortex clinging and big clinging) and big clinging cavities, are present behind impeller blades of Scaba turbine depending upon the gas flow rate and impeller rotational speed. The absence of big cavities was the possible reason for the lower drop in power consumption value in aerated condition and good gas dispersion efficiency. Moreover, the gas holdup, the mixing time and the mass transfer coefficient of the Scaba turbine are broadly equivalent to those of an equal-sized Rushton turbine for an equal power and superficial gas velocity (Nienow, 1998). These excellent characteristics of gas dispersion capability, power and mixing make the Scaba turbine an attractive alternative to the Rushton turbine for use in the process industry.

In recent years, significant work has been carried out to characterize the complex hydrodynamics near the rotating impeller blades for gas-liquid systems (Ranade et al., 2001 and Deen et al., 2002). In these studies, the Rushton turbine was used because of its simple shape and known flow characteristics. The prevailing flow near impeller blades is a complex function of the impeller size and shape. Therefore, the understanding of the flow generated by complex impellers and the capability to simulate the flow is essential for the design of impellers and the improvement of process performance in stirred vessels (Khopkar et al., 2004).

Little information about the flow generated by Scaba turbines is available in literature. Kovacs et al. (2001) measured and compared the discharge flow characteristics of the Scaba turbine and the Rushton turbine in single-phase flow using constant temperature hot wire anemometry (HWA). They observed similar bulk flow fields for both turbines, but in the case of the Scaba turbine, the turbulent kinetic energy and dissipation rate profiles had a sharp peak in the middle of the blade height. Regarding gas-liquid studies, there appears to be no such experimental data available for the flow in a stirred vessel equipped with a Scaba turbine.

CFD modelling has been shown to successfully simulate single-phase flow generated by impeller(s) of any shape in complex vessels (see for example, Ranade, 2002). The simulation of gas-liquid flow, however, exhibits significantly increased complexity. Despite such complexities, in recent years, several attempts have been made to develop computational models for gas-liquid flows in stirred vessels (Gosman et al., 1992; Bakker and Akker, 1994; Ranade and Akker, 1994; Morud and Hjertager, 1996; Lane et al., 1999; Lane et al., 2000 and Khopkar et al., 2003). All of these numerical studies concern the flow generated by either a Rushton turbine or a pitched blade turbine. To the authors' knowledge, work concerning the gas-liquid flow in a stirred reactor equipped with a Scaba turbine has not yet been reported in the literature.

In the present work, the gas-liquid flow generated by a Scaba turbine has been simulated using the approach reported by Khopkar et al. (2003). The angle resolved flow fields (liquid and gas-liquid flow) generated by the turbine have also been measured using PIV in order to better understand the flow around the blades for single phase, as well as gas-liquid flow. These experimental data, along with other reported data, are then used to validate the simulated results. A comparison of the flow fields generated by the Scaba and Rushton turbines is then made.

2. EXPERIMENTAL SET-UP

PIV measurements of instantaneous radial and axial liquid velocity components were carried out in a dished bottom fully baffled cylindrical vessel (of diameter, T = 0.19 m, height, H = 0.19 m, R_c = 0.19 m). Four baffles of width T/10 were mounted perpendicular to the vessel wall. The shaft of the impeller (d_s = 0.008 m) was extended to the bottom of the tank. A 6-blade Scaba turbine (of diameter, D_i = T/2 and impeller blade width, W = D_i/4) was used. The impeller off-bottom clearance was (C = T/3) measured from the bottom of vessel to the lowest horizontal plane swept by the impeller. The rotational speed of the impeller was set to 300 rpm, which is equivalent to an impeller Reynolds number (Re) of 45000. Gas was introduced into the vessel through a ring sparger of diameter 0.076 m. Experiments were carried out for a volumetric gas flow rate corresponding to a gas flow number of 0.004 (0.2 vvm, ug = 6.05×10^{-4} m/s).

Inherent limitations of particle image velocimetry (PIV) technique imposed some constraints on gas flow rates used in the present experiments. The accuracy of PIV system is dependant on the overall gas holdup value (Deen et al., 2002 and Delnoij, 1999). Deen et al. (2002) concluded that to obtain an accuracy of 90%, one has to keep the total gas holdup value less than 5 %. The high gas holdup behind impeller blades significantly reduces the accuracy of PIV measurements around the impeller blades. This limitation restricted us to a gas flow number of 0.004 (with overall gas hold up of about 1%) but enabled satisfactory measurements of the flow field around the impeller blades, which provide valuable whole field information, including the trailing vortices. Considering the role of trailing vortices on gas accumulation behind impeller blades and subsequently in the reduction in pumping capacity and power dissipation of impeller, the data presented in this work was found to be useful and adequate for evaluating the CFD model.

The PIV measurements were taken using a double-pulsed 30mJ:Mini YAG laser (Dantec Measurement Technology) having a variable frequency between 1 and 20Hz and a wavelength of 532nm (green). A CCD camera (Kodak Mega Plus ES 1.0) with a resolution of 1008×1018 pixels^2 was used to record simultaneous images of the flow. The thickness of laser sheet used was < 1 mm. An encoder, mounted on the impeller shaft, enabled synchronization of the image acquisition with the blade passage. The liquid was seeded using 30µm hollow glass particles with fluorescent rhodamine (Dantec Measurement Technology) implanted on the surface. The seeding (particle) density is one of the most important operational parameters and is one of the most common factors responsible for erroneous vectors. If the seeding density is too low, then there are not a sufficient number of particles available to statistically represent the flow, which results in a poor correlation calculation. In the present work, the amount of seeding introduced into the vessel was adjusted so that there were between 5 and 10 particles per interrogation area, as suggested by Bugay et al. (2002). This corresponds to a seeding particle concentration between 6 and 11 particles per cubic millimetre. These particles scatter light at a wavelength of 575nm which is greater than the wavelength of light scattered by air bubbles, 550nm. A filter was fitted to the camera, which enabled only light with a wavelength greater than 550nm to be captured. A schematic diagram of the experimental set-up is shown in Figure 1.

A PIV 2000 processor (Dantec Measurement Technology) and the commercial software package Flow Manager 3.40 (Dantec Measurement Technology) enabled synchronization of the camera and laser when necessary. Images were acquired at 15 Hz with an exposure time delay of 130 µs for the angle-resolved measurements and 300 µs for the mean flow field in the tank. Processing was then carried out using the software such that each image was divided up into interrogation areas of 32×32 pixels^2 (0.95×0.95 mm^2) with 50% overlap. A cross-correlation function in each area was then calculated using fast Fourier transforms (FFT) in order to determine the corresponding spatially averaged displacement vector. Before calculating the ensemble-averaged radial-axial velocity field for each impeller position or the mean global velocity field, every vector in each instantaneous velocity field was validated using a particular criterion. This criterion assumes that a vector is valid only if the signal

to noise (SNR) ratio (the ratio of the primary correlation peak to the second largest peak) is greater than 1.5 for single-phase measurements and 2.0 in the presence of gas. These thresholds has been previously applied and validated in stirred tank applications (Escudié, 2001 and Khopkar et al., 2003). Ensemble-averaged velocity fields were calculated using the valid vectors of 1000 instantaneous fields without gas and 1400 instantaneous fields with gas. Any non-valid vectors were not taken into account in this averaging. The angle resolved flow patterns were measured at six angles with respect to the centre-line of the blade: −10°, 0°, 10°, 20°, 30°, 40° and the global mean velocity field was taken in the mid-baffle plane.

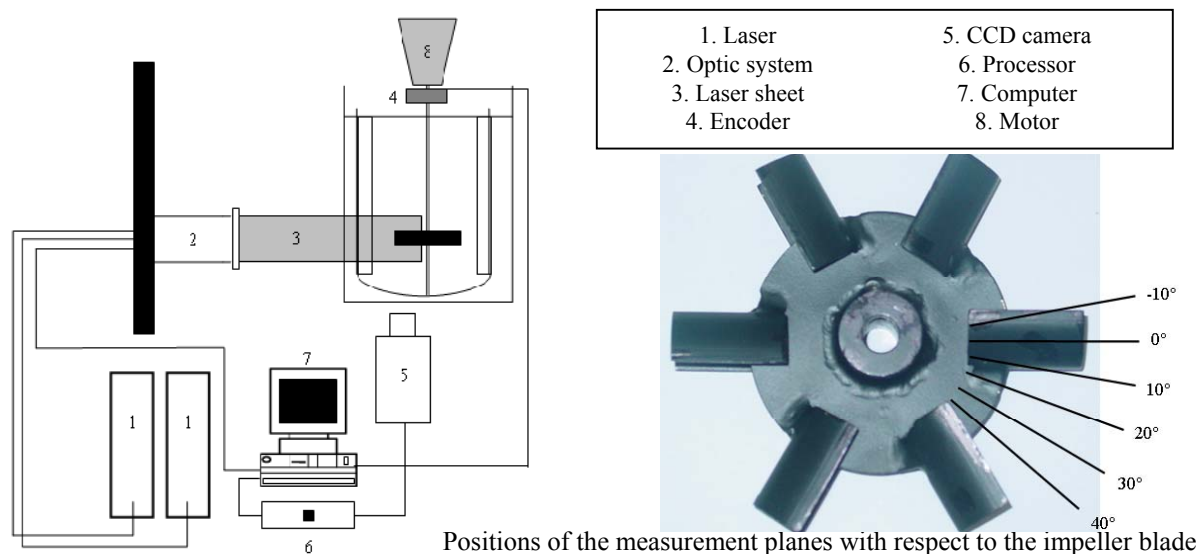| 1. Laser | 5. CCD camera |
2. Optic system	6. Processor
3. Laser sheet	7. Computer
4. Encoder	8. Motor

Positions of the measurement planes with respect to the impeller blade

Figure 1: Schematic Diagram of the Experimental Set-up and the Impeller

3. MATHEMATICAL MODELLING

3.1 Transport Equations

For simulating gas-liquid flow in the stirred vessel, a two-fluid model based on the Eulerian-Eulerian approach was used in this work. The mass and momentum balance equations for each phase may be written as:

$$\frac{\partial(\alpha_q \rho_q)}{\partial t} + \frac{\partial}{\partial x_i}\left(\alpha_q \rho_q U_{qi}\right) = 0 \tag{1}$$

$$\frac{\partial(\alpha_q \rho_q U_{qi})}{\partial t} + \frac{\partial}{\partial x_i}\left(\alpha_q \rho_q U_{qi} U_{qj}\right) = -\alpha_q \frac{\partial p}{\partial x_i} + \frac{\partial}{\partial x_i}\left(\alpha_q \mu_q\left(\frac{\partial U_{qj}}{\partial x_j} + \frac{\partial U_{qi}}{\partial x_i}\right)\right) +$$

$$\alpha_q \rho_q g_i + F_{qi} - \frac{2}{3}\frac{\partial}{\partial x_i}\left(\alpha_q \mu_q \frac{\partial U_{qm}}{\partial x_m}\right) \tag{2}$$

where U_{qi} is velocity of phase q in the i direction and F_{qi} is inter-phase momentum exchange term.

For most operating conditions, gas-liquid flow in stirred vessels is turbulent and the balance equations listed above (Equations 1 & 2) need to be time-averaged. Here, the conventional Reynolds averaging procedure has been used. For more details of time-averaged two-phase balance equations, the reader is referred to Ranade (2002). In the present work, turbulence in the dispersed two-phase flow was modeled by using the standard k-ε turbulence

model. The governing equations for the turbulent kinetic energy, k, and the turbulent energy dissipation rate, ε, were solved for the liquid phase only and are listed below:

$$\frac{\partial}{\partial t}\left(\rho_l \alpha_l k\right) + \frac{\partial}{\partial x_i}\left(\rho_l \alpha_l U_{li} k\right) = \frac{\partial}{\partial x_i}\left(\alpha_l \frac{\mu_t}{\sigma_k}\frac{\partial k}{\partial x_i}\right) + \alpha_l\left(G - \rho_l \varepsilon\right) \tag{3}$$

$$\frac{\partial}{\partial t}\left(\rho_l \alpha_l \varepsilon\right) + \frac{\partial}{\partial x_i}\left(\rho_l \alpha_l U_{li} \varepsilon\right) = \frac{\partial}{\partial x_i}\left(\alpha_l \frac{\mu_t}{\sigma_\varepsilon}\frac{\partial \varepsilon}{\partial x_i}\right) + \alpha_l \frac{\varepsilon}{k}\left(C_1 G - C_2 \rho_l \varepsilon\right) \tag{4}$$

where G is turbulence generation rate and μ_t is the turbulent viscosity:

$$G = \frac{1}{2}\mu_t\left(\nabla \overline{U} + \left(\nabla \overline{U}\right)^T\right)^2 \qquad \mu_t = \frac{\rho_l C_\varpi k^2}{\varepsilon} \tag{5}$$

Standard values of k-ε model parameters were used in the present simulations.

The interphase momentum exchange term consists of four different interphase forces: the Basset force, the virtual mass force, the lift force and the interphase drag force. In most cases, the magnitude of the Basset force is much smaller than that of the interphase drag force. In the bulk region of the vessel, the velocity gradients are small. However, near the impeller, the pressure gradients and the interphase drag forces mainly dominate the bubble motion. An order of magnitude analysis indicates that the magnitude of the lift force is much smaller than the interphase drag force Lane et al. (2000). Lane et al. (2000) showed that the effect of the virtual mass force is significant near the impeller blades and that in the bulk volume of vessel the effect diminishes. Considering this, only the interphase drag force was included in the interphase momentum exchange term in the present study. The inter-phase drag force exerted on phase 2 in the i direction is given by:

$$F_{q_i} = F_{D2i} = -\frac{3\alpha_1 \alpha_2 \rho_1 C_D\left(\sum\left(U_{2i} - U_{1i}\right)^2\right)^{0.5}\left(U_{2i} - U_{1i}\right)}{4d_b} \tag{6}$$

In gas-liquid stirred vessels, the interphase drag coefficient, C_D, is a complex function of the drag coefficient in a stagnant liquid, the gas holdup and prevailing turbulence. Lane et al. (2000) studied the effect of turbulence on the drag coefficient (via the slip velocity). Based on a comparison of the predicted gas volume fraction distribution with the experimental data, they recommended a turbulence correction factor base on that proposed by Brucato et al. (1998), but with a lower value of the correlation constant. Following this, the following correlation (Equation 7) for the calculation of the drag coefficient was used:

$$\frac{C_D - C_{D0}}{C_{D0}} = K\left(\frac{d_b}{\lambda}\right)^3 \tag{7}$$

$$C_{D0} = \max\left\{\left(\frac{2.667 * Eo}{Eo + 4.0}\right), \left(\frac{24}{Re_b} * \left(1 + 0.15 * Re_b^{0.687}\right)\right)\right\}$$

where λ is the Kolmogorov length scale, d_b is bubble diameter and K is the correlation constant with a value of 6.5×10^{-06}.

The gas-liquid flow in the stirred vessel was simulated using the computational snapshot approach. In this approach, the impeller blades are considered as fixed at one particular position (similar to taking a snapshot of rotating impeller) with respect to baffles. Recently Ranade (2002) discussed the development of snapshot approach in detail and therefore it is not repeated here. The flow is simulated for a specific blade position with respect to baffles. Results obtained with a specific snapshot were not found to be significantly different than the ensemble averages over a number of snapshots (Ranade and Akker, 1994). The computational snapshot approach was implemented in the commercial CFD code FLUENT 4.5 (of Fluent Inc., USA) using user-defined subroutines.

3.2 Solution Domain and Boundary Conditions

Considering the symmetry of the geometry, only half of the vessel was considered as a solution domain (see Figure 2). The baffles were considered at angles of 45° and 135°. The impeller was positioned in such a way that three blades were located at angles of 30°, 90° and 150° (measured from the center-line of the impeller blade). As discussed by Ranade (2002), the computational snapshot approach divides the solution domain into an inner region, in which time derivative terms are approximated using spatial derivatives and an outer region, in which time derivative terms are neglected. The boundary between the inner and outer regions needs to be selected in such a way that the predicted results are not sensitive to its actual location. In the present work, for all simulations, the boundary of the inner region was positioned at r = 0.064 m and 0.05 m ≤ z ≤ 0.15 m (where z is axial distance from the bottom of the vessel).

In the snapshot approach, the sparger is modeled as solid wall. The mass source of the gas phase was specified one cell above the sparger to simulate gas introduction into the vessel. Special boundary conditions are needed to simulate gas-liquid interface at the top through which bubbles escape the solution domain. Recently, Ranade (2002) has discussed the formulation of boundary conditions at the top surface of gas-liquid dispersion where gas bubbles leave the dispersion. Usual 'outlet' boundary condition, which specifies gradient normal to the outlet boundary as zero, cannot be applied for simulating gas-liquid flows because normal velocity of the liquid phase at the outlet boundary is zero. The top surface of gas-liquid dispersion is usually modelled in two ways, as free shear wall with gas sink, to remove gas from vessel, and as velocity inlet with normal outgoing gas velocity equal to terminal rise velocity of gas bubble and all other velocity components of gas and liquid phases were set to zero. In the present study the top surface of the liquid was modelled as velocity inlet. The presence of low liquid velocities ensures little effect on the predicted velocity field near top surface. The maximum difference in the predicted flow field by using both the boundary conditions was observed to be less than 10 %. The outgoing (axial) velocity of gas bubbles was set equal to the terminal rise velocity of gas bubbles (estimated as 0.2 m/s for air bubbles). Implicit assumption here is that gas bubbles escape the dispersion with terminal rise velocity. It should be noted that even after defining top surface as an inlet, gas volume fraction at the top surface is a free variable. The boundary condition used at the top surface of the vessel in this work represents a convenient way to represent this within the framework of commercial CFD code FLUENT. The mass and momentum conservation equations for the gas phase were solved and the gas distribution within the vessel was predicted. The mass conservation was verified by comparing the integral gas mass flow rate across various horizontal planes with the input gas mass flow rate at the sparger. The bubble diameter was set to 3×10^{-3} m for all the simulations. Fluid properties were set as those of water and air for primary and secondary phases, respectively.
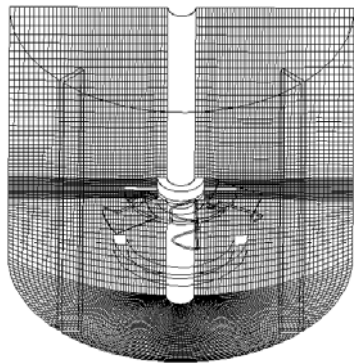
Grid Details	:
r × θ × z	: 52 × 95 × 67
Impeller blade	: 18 × 1 × 18
Inner region	: 13 ≤ k ≤ 55 j ≤ 40

Figure 2: Computational Grid and Solution Domain

A commercial grid-generation tool, GAMBIT 2.0 (Fluent Inc., USA) was used to model the geometry and to generate the body-fitted grids. It is very important to use an adequate number of computational cells while numerically solving the governing equations over the solution domain. The prediction of turbulence quantities is especially sensitive to the number of grid nodes and grid distribution within the solution domain. Our previous work Ranade et al., 2002, as well as other published work (Ng et al., 1998 and Wechsler et al., 1998) gives adequate information on the influence of the grid on the predicted results. It was demonstrated that, in order to capture the details of flow near impeller, it is necessary to use at least 200 grid nodes to resolve the blade surface. Based on

previous experience and some preliminary numerical experiments, the numerical simulations for gas-liquid flows in stirred vessels were carried out for a grid size of ($r \times \theta \times z$: $52 \times 95 \times 67$). In the present work we have used ($r \times \theta \times z$: $18 \times 1 \times 18$) grid nodes covering the impeller blade. The boundary of the inner region was positioned at $j \leq 40$ and $13 \leq k \leq 55$ (where j is the cell number in the radial direction from shaft and k is the cell number in the axial direction from bottom of vessel). The computational grid used in the present work is shown in Figure 2. Differencing of the advection terms has been carried using the QUICK discretization scheme with the SUPERBEE limiter function (to avoid non-physical oscillations). Standard wall functions were used to specify wall boundary conditions.

4. RESULTS AND DISCUSSION

4.1 Liquid-only Flow

The flow generated by the Scaba turbine in a stirred vessel was simulated for an impeller rotational speed of 300 rpm. Without using any impeller boundary conditions, the snapshot approach was able to simulate the flow generated by the impeller. The comparison of predicted velocity field of Scaba turbine (ensemble averaged to eliminate the influence of specific blade position) with the experimental PIV data (mid-baffle position) is shown in Figure 3. The radial velocity jet with two-loop flow structure (similar to Rushton turbine) seen in the experimental flow field is captured in the simulations. The simulated flow field shows two small re-circulating loops (attached to the inner edge of the impeller blades) below and above the disc. A small reverse loop below the hub, which is seen in the experimental flow field, is not however captured in the simulation. The predicted radial velocity field was used for calculating the flow (pumping) number for the Scaba turbine as:

$$N_Q = \frac{2 \int\limits_{-b/2}^{b/2} \int\limits_{0}^{\pi} \alpha_l r_i U_r \, d\theta \, dz}{N D_i^3} \qquad (8)$$

where b is the blade height, D_i is the impeller diameter, N is the impeller speed, r_i is the impeller radius and U_r is the radial velocity. The calculated value of the pumping number for the Scaba turbine from the simulated results (0.63) is higher than the experimental value determined by PIV (0.47) and that reported in the literature (0.52) [Kovacs et al., 2001].
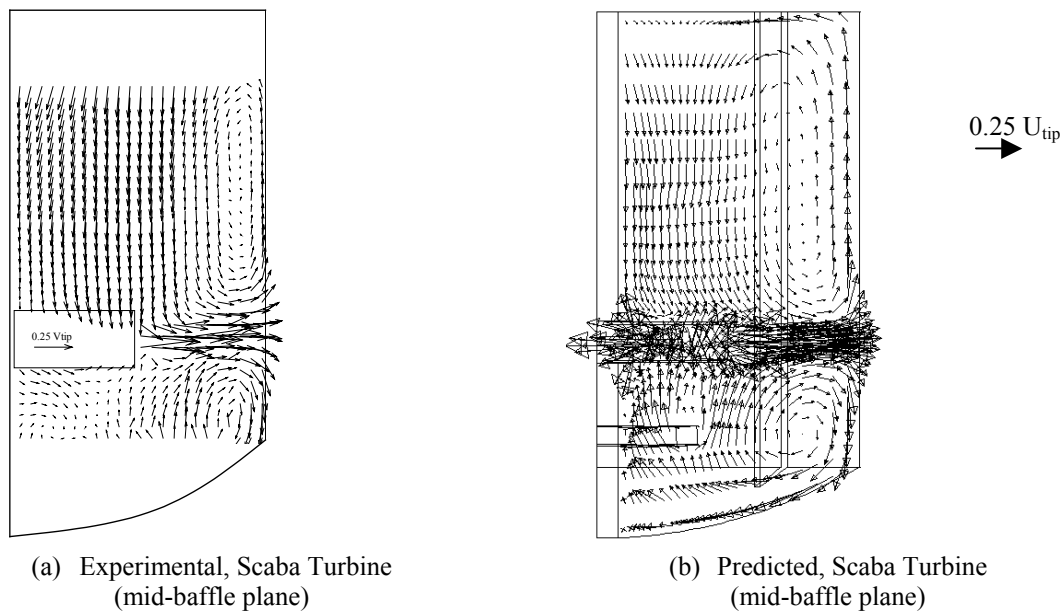

     (a)   Experimental, Scaba Turbine   (b)   Predicted, Scaba Turbine
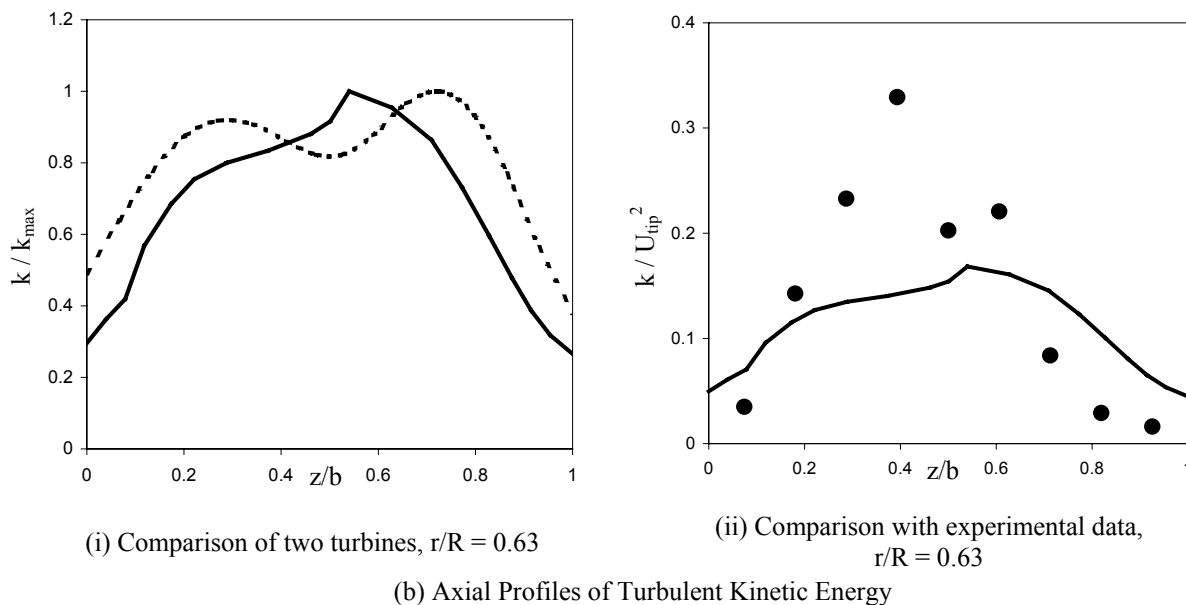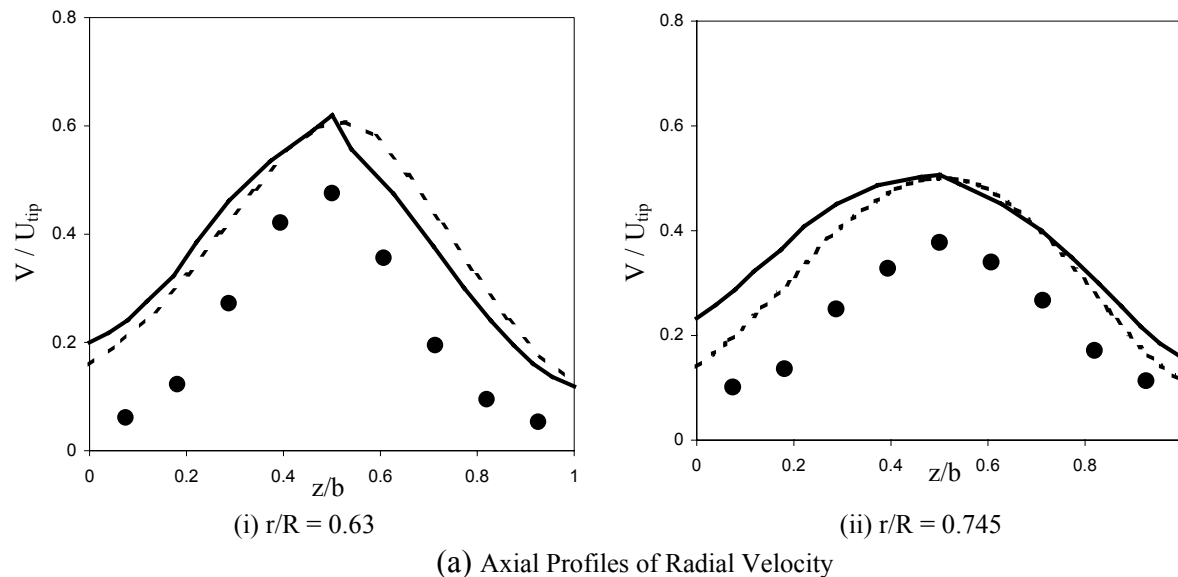   (mid-baffle plane)   (mid-baffle plane)

Figure 3: Mean Flow Field at the *r-z* Plane for Single-phase Flow, $N = 300$ rpm and $U_{tip} = 1.5$ m/s

In order to understand the effect of blade shape on flow, the flow generated by the Rushton turbine in a stirred vessel was simulated for the same geometry and for same grid resolution. The predicted flow fields were then used to identify the differences in flow field generated by these two turbines. To do this, the distribution of flow quantities around the impeller blade and along the blade height was analysed. The azimuthally averaged axial profiles of the predicted radial velocity and the turbulent kinetic energy for the two turbines are compared in Figure 4. It can be seen from Figures 4 (a) that despite the differences in the blade curvature of the two impellers, the azimuthally averaged velocity profiles do not differ significantly. The predicted profiles of the radial velocity almost overlap, although for the Scaba turbine, the predicted velocity profiles near the impeller tip show a well-defined peak at $z/b = 0.5$. When comparing the predicted values with the experimental data, it can be seen that the computational model over predicts the radial velocity values in the impeller discharge stream.

(i) r/R = 0.63   (ii) r/R = 0.745

(a) Axial Profiles of Radial Velocity

(i) Comparison of two turbines, r/R = 0.63

(ii) Comparison with experimental data,
r/R = 0.63

(b) Axial Profiles of Turbulent Kinetic Energy

Legends: —— Scaba turbine   - - - Rushton turbine   ● Experimental data of Scaba turbine

Figure 4: Comparison of Predicted Results with Experimental Data for Single-Phase Flow,
$N = 300$ rpm and $U_{tip} = 1.5$ m/s

The predicted turbulent kinetic energy distribution for both the turbines is shown in Figure 4 (b)-(i). It can be seen that the predicted distribution of kinetic energy (azimuthally averaged) in the impeller discharge stream is different for both turbines, highlighting the effect of blade shape. In the case of the Rushton turbine, two maxima at around $z/b = 0.25$ and 0.75 are observed. These observations have already been reported by other authors (Ng et al., 1998) and are related to the presence of trailing vortices. In the case of Scaba turbine, a sharp peak at $z/b = 0.54$ is observed. Kovacs et al. (2001) similarly reported a peak at $z/b = 0.5$. The comparison of predicted values with the experimental data shows that the computational model under predicts the turbulent kinetic energy values. This is a common finding when k-ε turbulence models are used. The use of more complex models, like Reynolds stress models, may not lead to any significant improvement (Jenne and Reuss et al., 1999). Recent work, however, shows that correct kinetic energy values in stirred tanks can be obtained via Large Eddy Simulations (LES) (Kilander and Rasmuson, 2003 and Yeoh et al., 2003). Such simulations, however, still require a significant amount of CPU time and therefore are not yet fine-tuned for fast process design. Nevertheless, the simulated results presented in this work enable correct qualitative comparisons between agitator types.

(a) Pressure Distribution around the Rushton Turbine
(10 uniform contours, blue ≡ -700, red ≡ 800)

(b) Pressure Distribution around the Scaba Turbine
(10 uniform contours, blue ≡ -2700, red ≡3800)

(c) Iso-surface of Z-Vorticity (L.H.S.: Scaba turbine and R.H.S.: Rushton turbine), $\omega D_i/U_{tip} = -30$
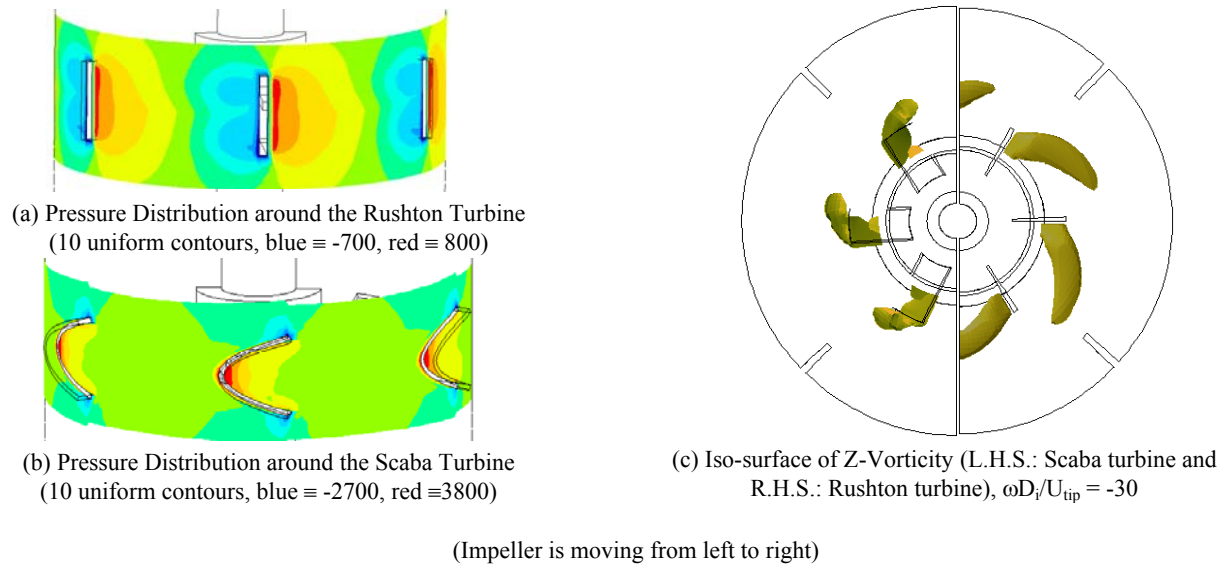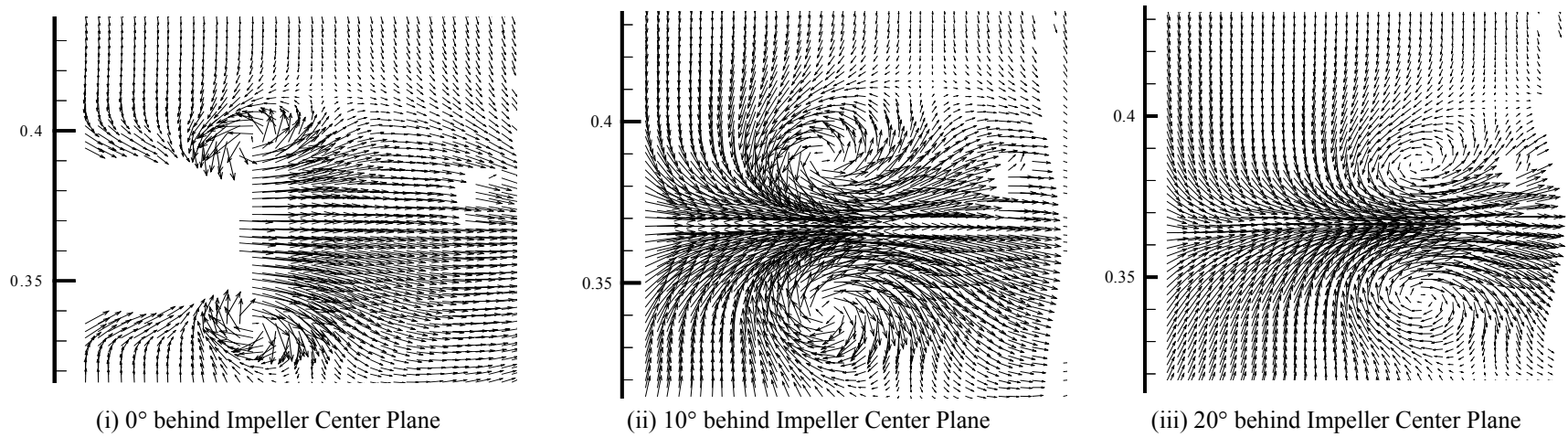
(Impeller is moving from left to right)

Figure 5: Flow Field around the Impeller Blades for Single-phase Flow, $N = 300$ rpm and $U_{tip} = 1.5$ m/s

To examine the flow structure around impeller blades, angle-resolved experimental data (obtained from PIV measurements) taken at 0°, 10° and 20° behind the centerline of the impeller blade are shown in Figure 6 (a). The presence of two trailing vortices and their radial movement away from the impeller as one moves further behind the blade are clearly evident. The PIV measurements show that the trailing vortices are clearly seen until at least 30° behind the impeller plane (results at 30° are not shown). The experimental turbulent kinetic energy contour plots for the Scaba turbine are shown in Figure 6 (b). Experimentally, the turbulent kinetic energy is determined using only two components of the velocity fluctuations in the *r-z* plane and is calculated using Equation 9:
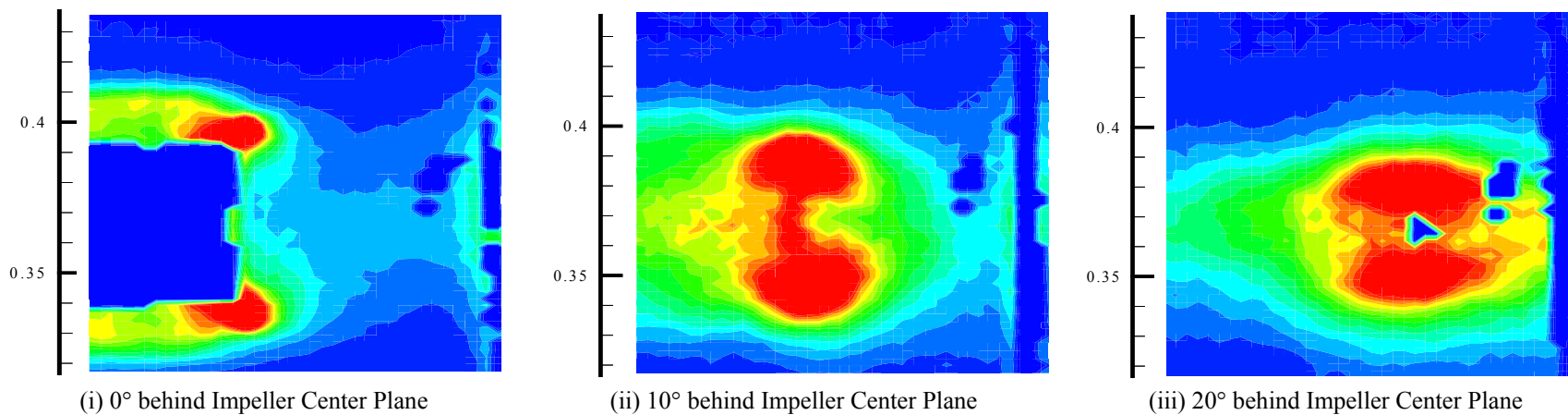
$$k = \frac{3}{4}\left(V'^2 + U'^2\right) \tag{9}$$

It can be seen that the two small trailing vortices are characterised by zones of increased turbulent kinetic energy. These zones of turbulent kinetic energy move radially away from the impeller as one moves further behind the blade.

The low-pressure regions generated behind the blades of the Scaba turbine and the consequent small low strength trailing vortices are the major reasons for the reduction of gas accumulation behind the impeller blades of this impeller and thus its improved performance compared with the Rushton turbine.

(i) 0° behind Impeller Center Plane (ii) 10° behind Impeller Center Plane (iii) 20° behind Impeller Center Plane

(a) Velocity Flow Field

(i) 0° behind Impeller Center Plane (ii) 10° behind Impeller Center Plane (iii) 20° behind Impeller Center Plane

(b) Turbulent Kinetic Energy Profiles (16 uniform contour plots, blue $\equiv$ 0.007 m^2/s^2 and red $\equiv$ 0.11 m^2/s^2)

Figure 6: Flow Field near the Impeller Blades (single flow), N = 300 rpm and U_{tip} = 1.5 m/s

4.2 Gas-liquid Flow

The gas-liquid flow generated by the Scaba turbine in the stirred vessel was simulated for a gas flow number of 0.004 and Froude number of 0.242. This corresponds to a volumetric gas flow rate (Q_g) of 1.715×10^{-5} m^3/s, superficial gas velocity (ug) of 6.05×10^{-4} m/s and an impeller rotational speed of 300 rpm. Under these operating conditions, the gas is completely dispersed in the vessel. The comparison of predicted liquid velocity field with the experimental PIV data at the mid-baffle plane is shown in Figure 7. Both the experimental and predicted velocity fields show a reduction in the liquid velocity magnitudes for the case of gas-liquid flow, compared with the liquid-only flow. The predicted radial velocity field is used for calculating the flow (pumping) number. The calculated value of pumping number from the simulated results (0.59) is higher than the measured experimental value of 0.44. The predicted gas holdup distribution at mid-baffle plane is shown in Figure 8 (a). It can be seen that the computational model captures the complete dispersion of gas in the vessel. The predicted gas holdup distribution shows higher values of gas holdup in the lower circulation loop, indicating recirculation of the gas in the lower part of the vessel.
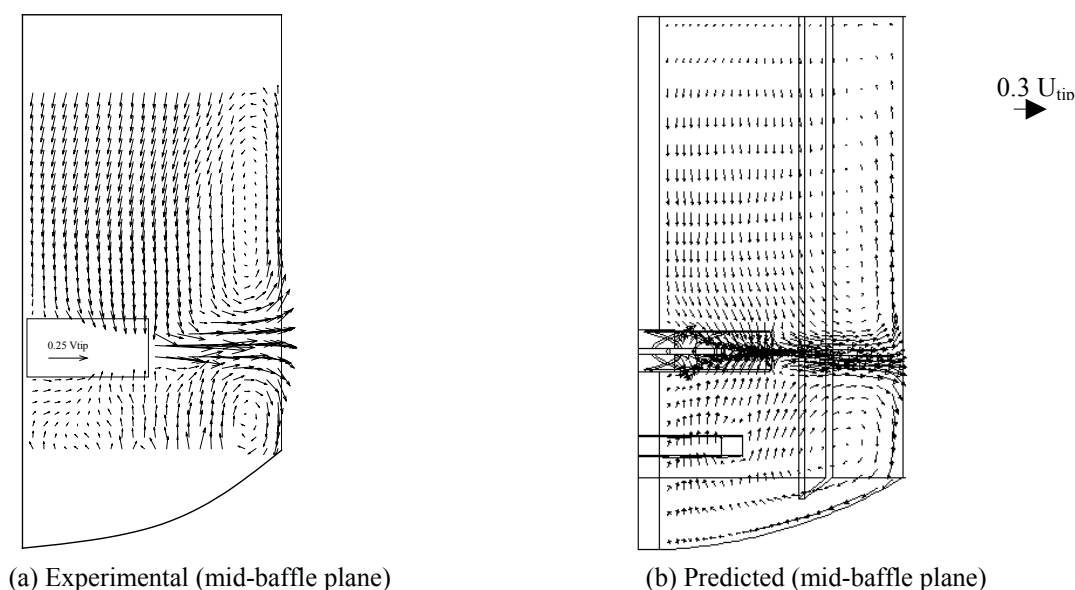

(a) Experimental (mid-baffle plane)   (b) Predicted (mid-baffle plane)

Figure 7: Mean Liquid Flow Field at the r-z Plane for Gas-Liquid Flow, Fl = 0.004, Fr = 0.242 and U_{tip}= 1.5 m/s

The computational model was further used to study the effect of the aeration rate on the gas dispersion performance of Scaba turbine. The gas-liquid flows in stirred vessel were simulated for two higher aeration rates (Fl = 0.04, ug = 6.05×10^{-3} m/s and Fl = 0.1, ug = 0.015 m/s), while the impeller speed was kept constant. The predicted gas holdup distribution for high gas loading (Fl = 0.1) is shown in Figure 8 (b). It can be seen that even for high gas loading, the Scaba turbine provides good dispersion of the gas and significant holdup in the lower circulation loop.

The angle-resolved velocity fields of the flow around the impeller blades obtained by PIV are shown in Figure 9 (a). The presence of the trailing vortices and their movement within the impeller stream are clearly evident from the velocity vector plots. Similar to the results of the liquid-only flow, the movement of trailing vortices in the gas-liquid flow is clearly seen up to at least 30° behind the blade. However, the strength of the trailing vortices is slightly damped in the presence of the gas and the vortex centers are further apart than the case without gas. The predicted gas holdup distributions around the impeller blades of the Scaba turbine for three gas flow rates are shown in Figure 9 (b). It can be seen that the computational model captures the gas accumulation behind the impeller blades. The sparged gas interacts with the lower trailing vortices and accumulates in the low-pressure region associated with the lower trailing vortex of each blade. This is confirmed by the experimental data shown in Figure 9 (a)-(ii): in the lower vortex, there is an absence of liquid velocity vectors, which indicates that gas is often present

in this zone. It is also observed that even at very high gas flow rates (Figure 9 (b)-(iii)) the gas accumulation structure and magnitude hardly change.
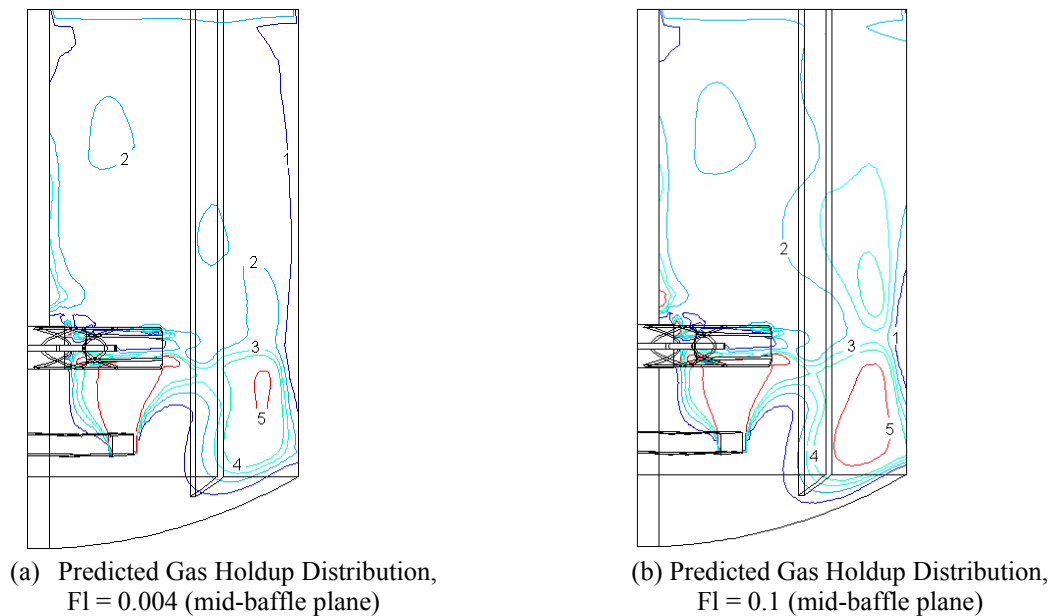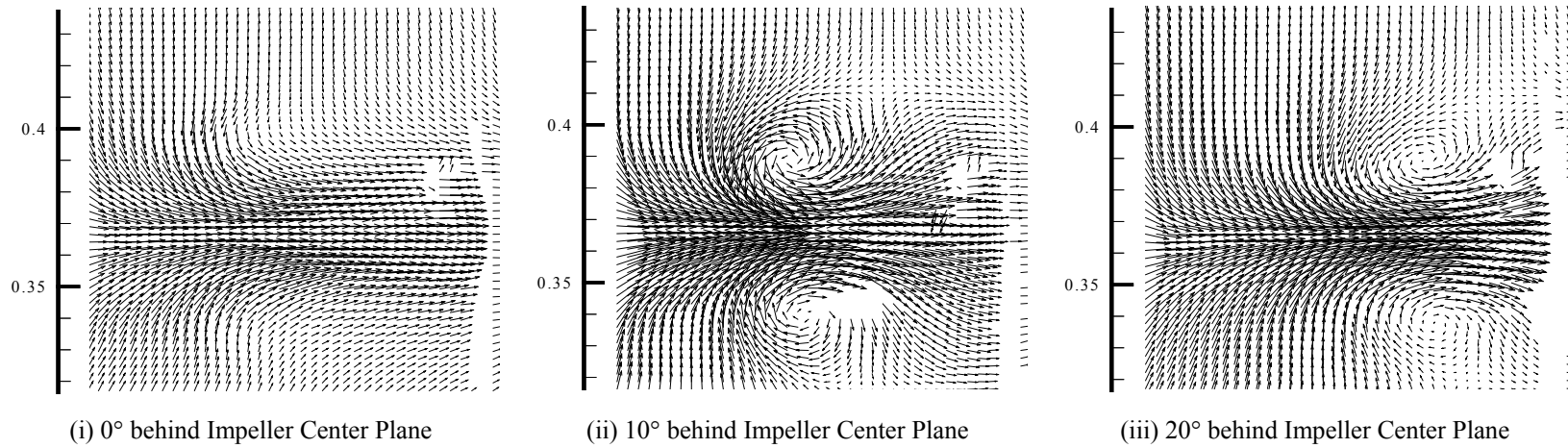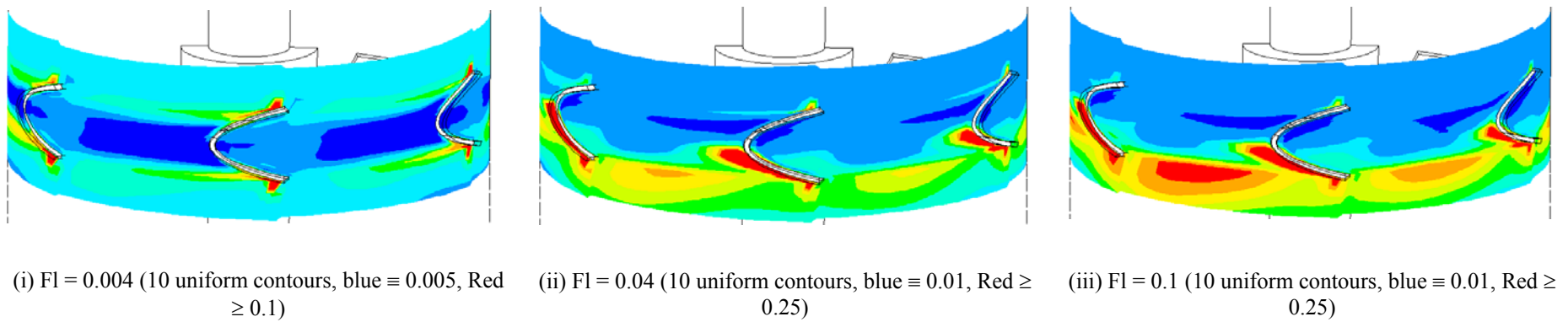

(a) Predicted Gas Holdup Distribution, Fl = 0.004 (mid-baffle plane)

(b) Predicted Gas Holdup Distribution, Fl = 0.1 (mid-baffle plane)

Figure 8: Predicted Gas Holdup Distribution at the r-z Plane for Gas-Liquid Flow, Fr = 0.242 and U_{tip}= 1.5 m/s (Contour labels denote the predicted values of gas holdup, in percentage)

The computational model was further used to study the effect of the aeration rate on the gas dispersion performance of Scaba turbine. The gas-liquid flows in stirred vessel were simulated for two higher aeration rates (Fl = 0.04, ug = 6.05×10^{-3} m/s and Fl = 0.1, ug = 0.015 m/s), while the impeller speed was kept constant. The predicted gas holdup distribution for high gas loading (Fl = 0.1) is shown in Figure 8 (b). It can be seen that even for high gas loading, the Scaba turbine provides good dispersion of the gas and significant holdup in the lower circulation loop.

The angle-resolved velocity fields of the flow around the impeller blades obtained by PIV are shown in Figure 9 (a). The presence of the trailing vortices and their movement within the impeller stream are clearly evident from the velocity vector plots. Similar to the results of the liquid-only flow, the movement of trailing vortices in the gas-liquid flow is clearly seen up to at least 30° behind the blade. However, the strength of the trailing vortices is slightly damped in the presence of the gas and the vortex centers are further apart than the case without gas. The predicted gas holdup distributions around the impeller blades of the Scaba turbine for three gas flow rates are shown in Figure 9 (b). It can be seen that the computational model captures the gas accumulation behind the impeller blades. The sparged gas interacts with the lower trailing vortices and accumulates in the low-pressure region associated with the lower trailing vortex of each blade. This is confirmed by the experimental data shown in Figure 9 (a)-(ii): in the lower vortex, there is an absence of liquid velocity vectors, which indicates that gas is often present in this zone. It is also observed that even at very high gas flow rates (Figure 9 (b)-(iii)) the gas accumulation structure and magnitude hardly change.

The little change in the quantity of the gas accumulation behind impeller blades for higher gas loading explains the so called advantages of Scaba turbine over the Rushton turbine for gas dispersion applications. The presence of small and clinging cavities ensures the less drop in pumping capacity and power dissipation of the impeller. These observations are valid for small and pilot plant scale vessels. However, for large or industrial scale vessel, the ratio of characteristic length scales of impeller blades and the gas bubble are strikingly different as compared to small vessel. Therefore, the interaction of gas bubbles with the trailing vortices and the structure of the cavities might be significantly different for industrial scale as compared to small vessel. Though some indirect evidence of this is available, to the author's knowledge no systematic study of influence of scale on relative performance of the Scaba turbine is available. We have initiated the CFD simulations to understand the influence of the scale on the relative performance of the Scaba turbine. These results will be reported separately.

(i) 0° behind Impeller Center Plane   (ii) 10° behind Impeller Center Plane   (iii) 20° behind Impeller Center Plane

(a) Liquid Velocity Flow Field (Experimental data), Fl = 0.004

(i) Fl = 0.004 (10 uniform contours, blue ≡ 0.005, Red ≥ 0.1)   (ii) Fl = 0.04 (10 uniform contours, blue ≡ 0.01, Red ≥ 0.25)   (iii) Fl = 0.1 (10 uniform contours, blue ≡ 0.01, Red ≥ 0.25)

(b) Predicted Gas Holdup Distribution around the Impeller Blades

Figure 9: Flow Field near the Impeller Blades (Gas-liquid flow), Fr = 0.242 and U_{tip}= 1.5 m/s

Analysis of comparison of the predicted results with the experimental data indicates that the major disagreement was observed in the impeller discharge stream. The computational model has over-predicted the liquid velocities and under-predicted the turbulent kinetic energy in impeller discharge stream. Ranade et al. (2002) and Khopkar et al. (2003) have also reported the similar observations. The quality of grid and inadequate understanding of physics are the two most possible reasons for the observed discrepancy. The number of grid nodes and the quality of grid used in impeller discharge stream significantly controls the accurate prediction of flow around impeller blades. For single-phase flow, the computational model with more than 200 cells on impeller blade face and higher order discretization scheme was found to be adequate for the accurate prediction of the velocity distribution in the impeller discharge stream for simple impellers like Rushton turbine (Ranade et al., 2002). Even for such cases, the turbulent kinetic energy in the impeller discharge stream was under-predicted. The use of standard k--ε turbulence model is one the possible reasons for the under-prediction of the turbulent kinetic energy. Jenne and Reuss (1999) used different turbulence models for simulating liquid flow in a baffled stirred vessel. This as well as other studies indicated that though agreement in some of the regions was found to improve by use of a variant of the standard k-ε model, agreement in some other region of the vessel was found to deteriorate. Thus it was not possible to evolve a conclusive recommendation about the turbulence model. Large eddy simulations (LES) were found to improve the agreement to some extent (see discussion in Ranade, 2002). However use of LES for simulating gas-liquid flows requires enormous computational resources and its benefits for simulating gas-liquid flow has not yet been demonstrated. It was therefore not used in the present work.

Apart from the grid and choice of turbulence model, the accuracy and the reliability of simulations of gas-liquid flow in stirred vessels depend upon the specified bubble size; used inter-phase drag model and the modelling of gas cavities behind impeller blades. In gas-liquid stirred vessel very fine bubbles are observed in impeller discharge stream and the bubble size varies non-homogeneously between 700 μm to 5 mm (Barigou and Greaves, 1992) depending upon the turbulence level and prevailing flow regime. It is in principle possible to use population balance model with appropriate breakage and coalescence rates (see for example, Buwa and Ranade, 2002) to account for bubble size distribution within the vessel. However, this increases the demands on computational resources by an order of magnitude. More importantly, the right parameters of the underlying coalescence and breakage kernels are often unavailable. Therefore, population balance models were not considered in the present work. The use of a single bubble diameter may be one of the reasons for observed discrepancies. The numerical studies of Khopkar and Ranade (2004) explained the importance of correct modelling of drag force. The drag force in stirred vessel is a complex function of drag coefficient in a stagnant liquid, gas holdup and prevailing turbulence. In present study, we have used the correlation proposed by Brucato et al. (1998), with a modified value of the proportionality constant to simulate the effect of turbulence on drag coefficient. Although, the predicted results are in reasonable agreement with the experimental data, further investigations to evolve a more generalized inter-phase drag force model are needed. The present computational model does not account for the actual shape and size of the cavity. This may lead to over-prediction of the velocity values in impeller discharge stream for gas-liquid systems. Further work on methodology of modeling cavities behind blades is needed to improve predictive abilities of CFD models.

Despite some of the limitations discussed above, the approach and models similar to those used here were used by Khopkar et al. (2004) and Khopkar and Ranade (2004) to predict the gas-liquid flow generated by the Rushton turbine in different gas flow regimes, such as vortex clinging, 3-3 and flooding. The comparison of the predicted liquid velocity distribution and the gas holdup distribution with the measured and previously reported data was reasonably good. The computational model was able to predict the gas dispersion in different regime and specifically inability of impeller to disperse the gas in liquid bulk for the flooding regime. The model was also shown to capture accumulation of gas behind impeller blades and reduction in power dissipation in presence of gas reasonably well. However, the computational model did not predict the asymmetry in the cavity size for 3-3 cavity structure. Considering this, the presented approach and computational model is useful to capture key features of gas-liquid flow in stirred vessels and therefore can be used for engineering decision-making.

5. CONCLUSIONS

PIV and CFD simulations were used to study the gas-liquid flow generated by a 6-blade Scaba turbine. Angle resolved PIV measurements (velocity fields and contours of kinetic energy) clearly show the presence of two trailing

vortices behind each impeller blade for single phase, as well as gas-liquid flow. The trailing vortices were found to retain their structure up to about 30° behind the impeller blade. In the presence of gas, however, the strength of the trailing vortices is slightly lower and they are further apart.

The CFD simulations have enabled the similarities and the differences between the single-phase flows generated by the Rushton and Scaba turbines to be identified. The computational model correctly captures the overall flow field generated by both the turbines. The predicted results also indicate a difference in the axial profiles of velocities, which show decay as one move away from the impeller tip plane. The difference between the shapes of the axial profiles of turbulent quantities for the two turbines is significant and is related to the strength and size of the trailing vortices generated by the different impellers. Gas-liquid flow in the stirred vessel was simulated for three gas flow rates (Fl = 0.004, Fl = 0.04 and Fl = 0.1). With respect to the gas phase, the computational model was able to capture the complete dispersion of the gas. Overall, the model appears to capture most of the key features of the single phase, as well as the gas-liquid flow, including the presence of the trailing vortices and the accumulation of gas behind the impeller blades. The results of the CFD simulations are in reasonably good agreement with the experimental data. The model and the approach presented here may be used for engineering decision making. Future work will focus on the improvement of the CFD model by incorporating better sub-models of (1) drag force, (2) cavities behind blades and (3) bubble size distribution.

ACKNOWLEDGEMENTS

NOTATIONS

b : impeller blade height, m
C : impeller off-bottom clearance, m
C_D : drag coefficient
C_{D0} : drag coefficient in stagnant water
C_ω : constant
d_b : bubble diameter, m
D_i : impeller diameter, m
d_s : impeller shaft diameter, m
Eo : Evotos number
F_q : interphase momentum exchange term
F_D : interphase drag force, N/m^3
g : acceleration due to gravity, m/s^2
G : turbulence generation rate
H : vessel height, m
k : turbulent kinetic energy, m^2/s^2
K : constant
N : impeller rotational speed, rps
Q_g : volumetric gas flow rate, m^3/s
r : radial coordinate, m
R_c : curvature of vessel bottom, m
T : vessel diameter, m
t : time, s
U : axial velocity, m/s
U_{tip} : impeller tip speed, m/s
V : radial velocity, m/s
x : position vector, m

z : axial coordinate, m

Greek Symbols
α : gas volume fraction
ε : turbulent kinetic energy dissipation rate, m^2/s^3
λ : Kolmogorov length scale, m
ρ : density, kg/m^3
$\sigma_{\varepsilon,k}$: constants in k-ε turbulence model
μ : viscosity, kg/ms
ϕ : scalar variable
θ : tangential coordinate
ω : Z-vorticity

Dimensionless numbers
Fl   : flow number
Fr   : Froude number
N_P : power number
N_Q : pumping number
Re   : impeller Reynolds number
Re_b : bubble Reynolds number

Subscripts
1   : liquid
2   : gas
q : phase number
t : turbulent

Superscript
`   : rms value

REFERENCES

Bakker, A. and van den Akker, H.E.A., "A computational model for the gas-liquid flow in stirred reactors", Trans IChemE, Vol. 72, 594- 606 (1994).

Barigou, M. and Greaves, M., "Bubble size distribution in a mechanically agitated gas-liquid contactor", Chem. Engg. Sci., Vol. 47, 2009-2025 (1992).

Brucato, A., Grisafi, F. and Montante, G., "Particle drag coefficient in turbulent fluids", Chem. Eng. Sci., Vol. 45, 3295-3314 (1998).

Bugay, S.; Escudié, R. and Liné, A., "Experimental Analysis of Mean Flow and Turbulence Structure in Agitated Tank Based on PIV Technique with Axial Impeller", AIChE J., Vol. 48, 463 (2002).

Bruijn, W., Van't Riet, K and Smith, J.M., "Power consumption with aerated Rushton turbines", Trans. I. Chem. E., Vol. 52, 88 (1974).

Buwa, V.V. and Ranade, V.V., "Dynamics of gas-liquid flow in rectangular bubble columns", Chem. Eng. Sci., Vol. 57, 4715-4736 (2002).

Deen, N.G., Solberg, T. and Hjertager, B. H., "Flow generated by an aerated Rushton impeller, Part I: two-phase PIV experiments", Can. J. Chem. Eng., Vol. 80, 1-15 (2002).

Delnoij, E., "Fluid dynamics of gas-liquid bubble columns", Ph.D. Thesis, University of Twente, (1999).

Escudié R., "Structure Locale de l'Hydrodynamique Generée par une Turbine de Rushton", Ph.D. Thesis, INSA, Toulouse (2001).

Gosman, A.D., Lekakou, C., Politis, S., Issa, R.I. and Looney, M.K., "Multi-dimensional modeling of turbulent two-phase flows in stirred vessels", AIChEJ, Vol. 38, 1947-1956 (1992).

Jenne, M. and Reuss, M., "A critical assessment on the use of k-ε turbulence model for simulation of turbulent flow induced by a Rushton turbine in a baffled stirred tank reactor", Chem. Eng. Sci., Vol. 54, 3921-3941 (1999).

Khopkar, A.R., Aubin, J., Xureb, C., Le Sauze, N., Bertrand, J. and Ranade, V.V., Gas-liquid flow generated by a pitched blade turbine: PIV measurements and CFD simulations, Ind. Eng. Chem. Res., Vol. 42, 5318-5332 (2003).

Khopkar, A.R., Mavros, P., Ranade, V.V. and Bertrand, J., "Simulation of flow generated by an axial flow impeller: Batch and continuous operation", Chem. Eng. Res. Des., Vol. 82, 737-751 (2004).

Khopkar, A.R., Rammohan A., Dudukovic, M.P. and Ranade, V.V., "Gas-liquid flow generated by a Rushton turbine: CARPT/CT measurements and CFD simulations", presented at ISMIP 5, held at Spain, June (2004).

Khopkar, A.R. and Ranade, V.V., "CFD simulation of gas-liquid flow in stirred vessels: VC, S33 and L33 flow regimes", in preparation (2004).

Kilander, J. and Rasmuson, A., "Hydrodynamics in a stirred square tank investigated using a 3D PIV LES decomposition approach and LDA measurements", in Proc. of the 11th European Conference on Mixing, Bamberg, 31-38 (2003).

Kovacs, T., Tragardh, C. and Fuchs, L., "Flow and turbulence in the discharge of radial pumping turbines: influence of the turbine type", Chem. Eng. Tech., Vol. 24, 1035-1044 (2001).

Lane, G. L., Schwarz, M. P. and Evans, G. M., "CFD simulations of gas-liquid flow in a stirred tank", Proc. 3rd Int. Sym. on Mixing in Industrial Processes, Osaka, Japan, 21-28 (1999).

Lane, G. L., Schwarz, M. P. and Evans, G. M., "Modelling of the interaction between gas and liquid in stirred vessels", 10th European Conference on Mixing, 197-204 (2000).

Morud, K.E and Hjertager B.H., "LDA measurements and CFD modelling of gas-liquid flow in stirred vessel", Chem. Eng. Sci., Vol. 51, 233-249 (1996).

Nienow, A.W., Wisdom, D.J., and Middleton, J.C., "The effect of scale and geometry on flooding, recirculation and power in gassed stirred vessels", Proceedings of the Euro. Conf. On Mixing, Paper F1, Cambridge (1977).

Nienow, A.W., "Gas dispersion performance in fermenter operation", Chem. Eng. Prog., Vol. 86, 61-71 (1990).

Nienow, A.W., "Hydrodynamics of stirred bioreactors", Appl. Mech. Rev., Vol. 51, 3-32, (1998).

Ng, K., Fentiman, N. J., Lee, K.C. and Yianneskis, M., "Assessment of sliding mesh CFD predictions and LDA measurements of the flow in a tank stirred by a Rushton impeller", Chem. Eng. Res. Des., Vol. 76, 737-747 (1998).

Ranade, V.V. and van den Akker, H.E.A., "A computational snapshot of gas-liquid flow in baffled stirred reactors", Chem. Eng. Sci., Vol. 49, 5175-5192 (1994).

Ranade, V.V., Perrard, M., Xureb, C., Le Sauze, N. and Bertrand, J., "Influence of gas flow rate on the structure of trailing vortices of a Rushton turbine", Chem. Eng. Res. Des., Vol. 79A, 957-964 (2001a).

Ranade, V.V., Tayaliya, Y. and Krishnan, H., "CFD predictions of flow near impeller blades in baffled stirred vessels: assessment of computational snapshot approach", Chem. Eng. Comm., Vol. 189, 895-922 (2002).

Ranade, V.V., "Computational Flow Modeling for Chemical Reactor Engineering", Academic Press, New York (2002).

Saito, F., Nienow, A.W., Chatwin, S. and Moore, I.P.T., "Power, gas dispersion and homogenisation characteristics of Scaba SRGT and Rushton turbine impellers", J. Chem. Eng. Japan, Vol. 25, 281-287 (1992).

Van't Riet, K., Boom, J.M. and Smith, J.M., "Power consumption, impeller coalescence and recirculation in aerated vessel", Trans I Chem E., Vol. 54, 124-131 (1976).

Wechsler, K., Breuer, M. and Durst, F., "Steady and unsteady computations of turbulent flows induced by a 4/45° pitched blade impeller", J. of Fluids Eng., Vol. 121, 318 (1999).

Yeoh, S.L., Papadakis, G. and Lee, K.C., "Large eddy simulation of turbulent flow in Rushton impeller stirred reactor with a sliding-deforming mesh methodology", in Proc. of the 11th European Conference on Mixing, Bamberg, 39-46 (2003).